

BRNO UNIVERSITY OF TECHNOLOGY

VYSOKÉ UČENÍ TECHNICKÉ V BRNĚ

FACULTY OF MECHANICAL ENGINEERING

FAKULTA STROJNÍHO INŽENÝRSTVÍ

INSTITUTE OF PHYSICAL ENGINEERING

ÚSTAV FYZIKÁLNÍHO INŽENÝRSTVÍ

REAL-TIME STUDY OF REACTION WAVES

STUDIUM REAKČNÍCH VLN V REÁLNÉM ČASE

BACHELOR'S THESIS

BAKALÁŘSKÁ PRÁCE

AUTHOR AUTOR PRÁCE Richard Gazdík

SUPERVISOR

Ing. Petr Bábor, Ph.D.

VEDOUCÍ PRÁCE

BRNO 2022



Assignment Bachelor's Thesis

Institute: Institute of Physical Engineering

Student: Richard Gazdík

Degree programme: Physical Engineering and Nanotechnology

Branch: no specialisation

Supervisor: Ing. Petr Bábor, Ph.D.

Academic year: 2021/22

As provided for by the Act No. 111/98 Coll. on higher education institutions and the BUT Study and Examination Regulations, the director of the Institute hereby assigns the following topic of Bachelor's Thesis:

Real-time study of reaction waves

Brief Description:

The bachelor thesis will study the oxidation of carbon monoxide on the surface of platinum. The aim of the thesis is to observe the reaction waves that occur during the oxidation of carbon monoxide on the platinum surface to form carbon dioxide by SEM (Scanning Electron Microscopy) and AFM (Atomic Force Microscopy) in real time. The observations will be carried out first using an ultra—high vacuum electron microscope (UHV—SEM) and then the experiment will be transferred to a high vacuum electron microscope (HV—SEM) equipped with Nenovision AFM equipment.

Bachelor's Thesis goals:

- 1. Make observations of the reaction waves during the oxidation of carbon monoxide on platinum using UHV-SEM.
- 2. Transfer the experiment from step 1 to an HV-SEM equipped with an AFM microscope. Here, try to make correlative observations of the reaction waves using the CPEM (Correlative Probe and Electron Microscopy) method.

Recommended bibliography:

VAN SPRONSEN, Matthijs A., Joost W.M. FRENKEN a Irene M.N. GROOT. Surface science under reaction conditions: CO oxidation on Pt and Pd model catalysts [online]. 2017. ISSN 14604744. Dostupné z: doi:10.1039/c7cs00045f

PERILLI, Daniele, Sara FIORI, Mirco PANIGHEL, Hongsheng LIU, Cinzia CEPEK, Maria PERESSI, Giovanni COMELLI, Cristina AFRICH a Cristiana DI VALENTIN. Mechanism of CO Intercalation through the Graphene/Ni(111) Interface and Effect of Doping. The journal of physical chemistry letters [online]. 2020, 11(20), 8887–8892. ISSN 19487185. Dostupné z: doi:10.1021/acs.jpclett.0c02447

Deadline for submission Bachelor's Thesis is given by the Schedule of the Academic year 2021/22

In Brno,

L. S.

prof. RNDr. Tomáš Šikola, CSc.
Director of the Institute

Director of the Institute

Director Schedule of the Academic year 2021/22

L. S.

doc. Ing. Jaroslav Katolický, Ph.D.
FME dean

JAKUBITH, S., H. H. ROTERMUND, W. ENGEL, A. VON OERTZEN a G. ERTL. Spatiotemporal concentration patterns in a surface reaction: Propagating and standing waves, rotating spirals, and turbulence. Physical Review Letters [online]. 1990, 65(24), 3013–3016. ISSN 00319007. Dostupné

z: doi:10.1103/PhysRevLett.65.3013

Abstract

This bachelor's thesis is concerned with the heterogeneous catalytic oxidation of carbon monoxide, and especially with the reaction waves occurring under certain conditions, on the surface of platinum. The thesis is separated into two main parts - theoretical and experimental. The theoretical part provides information regarding the scanning electron microscope, the atomic force microscope and the details of the reaction. For the experimental part, the observation of this reaction was done both in an ultra-high vacuum and in a high vacuum scanning electron microscope, for both of which the reaction waves were identified. The goal was to also try to carry out a correlative probe and electron microscopy (CPEM) measurement of the reaction waves, which, unfortunately, for many reasons described in the last part of the thesis, was not successful.

Keywords

SEM, AFM, CO oxidation, heterogeneous catalytic reaction, reaction waves

Abstrakt

Táto bakalárska práca sa zaoberá heterogénnou katalytickou oxidáciou oxidu uhoľnatého, a hlavne reakčnými vlnami vyskytujúcimi sa pri určitých podmienkach, na povrchu platiny. Práca je rozdelená na dve hlavné časti – teoretickú a experimentálnu. Teoretická časť podáva informácie ohľadom rastrovacieho elektrónového mikroskopu, mikroskopu atomárnych síl a detailov reakcie. Pre experimentálnu časť boli vykonané pozorovania tejto reakcie v ultravysoko-vákuovom, ako aj vo vysoko-vákuovom rastrovacom elektrónovom mikroskope, a v oboch prípadoch boli identifikované reakčné vlny. Cieľom bolo tiež skúsiť vykonať korelatívne meranie reakčných vĺn sondou a elektrónovým mikroskopom (CPEM), ktoré, bohužiaľ, z veľa rôznych dôvodov popísaných v poslednej časti práce, nevyšlo.

Kľúčové slová

SEM, AFM, CO oxidácia, heterogénna katalytická reakcia, reakčné vlny

GAZDÍK, Richard. *Real-time study of reaction waves*. Brno, 2022. Bachelor's thesis. Brno University of Technology, Faculty of Mechanical Engineering. Supervised by Petr BÁBOR



Acknowledgements

I would like to thank my supervisor Ing. Peter Bábor, PhD. for his guidance and help on this thesis. My thanks also go to Bc. Dominik Hrůza and Bc. Antonín Jaroš for their help and discussions concerning the UHV-SEM measurements. I am grateful to Ing. Karel Vařeka for his help and work done regarding the HV-SEM measurements and AFM operation. I am thankful to the Institute of Physical Engineering for the instruments provided to me. Last but not least, I thank my family and friends for their support during my studies.

CzechNanoLab project LM2018110 funded by MEYS CR is gratefully acknowledged for the financial support of the measurements/sample fabrication at CEITEC Nano Research Infrastructure.

Richard Gazdík

Contents

Intr	oduction	ו	3
1	Theo	pretical part	5
	1.1	Scanning electron microscope	
		1.1.1 Construction of SEM	
		1.1.2 SEM imaging	7
	1.2	Atomic force microscope	10
		1.2.1 Basic working principle of AFM	
		1.2.2 Contact mode	
		1.2.3 Dynamic modes	
	1.3	Heterogeneous catalytic CO oxidation	
		1.3.1 Reaction mechanism	
		1.3.2 Reaction rate oscillations	
		1.3.3 Spatiotemporal patterns	
		1.3.4 Spatiotemporal self-organization	18
2 E	Expe	erimental part	19
	2.1	Apparatus and sample	19
		2.1.1 Sample preparation	
		2.1.2 Ultra-high vacuum SEM	
		2.1.3 High vacuum SEM + AFM	
	2.2	UHV-SEM reaction	22
2	2.3	HV-SEM reaction + AFM	25
		2.3.1 HV-SEM reaction	
		2.3.2 AFM	28
Coı	nclusion		31
Ref	ferences	S	33
List	t of abbr	eviations	35

Introduction

The oxidation of carbon monoxide on the surface of platinum-group metals is, conceptually, a very simple reaction and has already been studied extensively ever since the 1970s. Nevertheless, its continuing importance is reflected in the steady increase of the number of articles concerning it every year [1]. This reaction mainly occurs in the catalytic converter of every automobile. Its scientific significance is, however, a lot more far-reaching than that. The description and explanation of the phenomena, which are common for reactions happening away from the equilibrium and are present also in this reaction, can be useful in the understanding of various other reactions or conditions, under which these reactions can occur.

The observations, which will be discussed in this thesis, are done on so-called model catalysts, which are simplifying some aspects of the catalysts used in real-life applications. Such catalysts are useful to be able to focus only on the most fundamental interactions of the reactants with the catalyst, leading to an understanding of the reaction at hand [1]. With this knowledge, more efficient catalysts, able to be used in e.g., catalytic converters, the production of fertilizers or possibly in the functioning of new batteries, can be synthesized. This is increasingly important as the need to lower emissions to combat climate change is becoming more wide-spread and apparent.

The goal of this thesis is to observe a particular mode of the catalytic oxidation of CO, in which reaction waves of the reactants are moving on the platinum surface. This is to be performed in an ultra-high vacuum and in a high-vacuum scanning electron microscope. Additionally, a correlative probe and electron microscopy (CPEM) measurement of the reaction waves, adding an atomic force microscope to the mix, is to be attempted.

1 Theoretical part

1.1 Scanning electron microscope

For many centuries, scientists had to rely mainly on their eyes to receive information about the world around us. Later, the optical microscope was invented to examine various objects which were too small for a human eye to observe. Eventually, even the limitations of light microscopy became evident – the inability to resolve objects of sizes close to its wavelength (known as the diffraction limit). This problem was solved, or at least pushed back further, with the invention of the first electron microscope.

According to de Broglie, every object has its associated wavelength. Electrons can therefore be regarded as waves with a wavelength λ derived from de Broglie's formula:

$$\lambda = \frac{h}{p} = \frac{h}{\sqrt{2mE_k}} = \frac{h}{\sqrt{2meU}},\tag{1.1}$$

where h is the Planck constant, p is the electron's momentum, m is its mass, E_k is its kinetic energy, e is the elementary charge and U is the accelerating voltage. In this formula, we assume a non-relativistic electron, which is accelerated by an electric potential difference U. From this formula we can calculate that even an electron with energy $E_k = 1 \text{ eV}$ has a wavelength $\lambda \sim 1 \text{ nm}$. By increasing U we can get electrons with even smaller wavelengths. Unfortunately, the electron's wavelength is not the limiting factor in improving the resolution in an electron microscope (spot size is) as will be described in part 1.1.1.

1.1.1 Construction of SEM

The SEM can be divided into two main parts: column and chamber. The column is where the electron gun and optical system is, while the sample holder and detector can be found in the chamber.

There are three types of electron guns that are commonly used in an SEM: thermionic emission gun (TEG), field emission gun (FEG) and Schottky emission electron gun (SEG), which is a combination of the former two. There are various reasons for using the different electron guns even though they have the same purpose - release electrons into the vacuum.

The TEG uses a so-called hot cathode (usually tungsten filament) that is heated to high temperatures (up to 2800 K) [2] by current passing through it. This gives some electrons enough energy to overcome the work function W and escape the filament completely. These electrons are heading in all directions and so need to be focused by a Wehnelt electrode (which has a negative potential) into a narrow beam. The smallest part of the beam is called a crossover, which for all intents and purposes, is considered as the actual electron source.

The FEG uses a so-called cold cathode. The cathode can again be a tungsten wire, but now a single crystal of tungsten with a small radius of curvature is attached to the wire. An extracting electrode creates a high electric field around this setup called an emitter. This makes some electrons be able to escape from the emitter by the tunnelling effect [2]. These electrons are much

more compact in the direction of the tip and so do not need to be focused by a Wehnelt.

The SEG uses a hot cathode and also an extracting voltage. The emitter is now coated with ZrO which reduces the work function of tungsten, enabling a high emission current at a lower temperature than in TEG. Both the FEG and SEG must be kept at a higher vacuum than is the case for TEG, because the emitter must be kept very clean in order to work properly [2].

The escaped electrons from the electron gun are then accelerated by a potential difference between the cathode and anode which can range from 0.1 keV up to 50 keV. The diameter of the crossover at this point is of the order of 10-50 µm for TEG and 10-100 nm for FEG and SEG [3].

To achieve a better resolution, the electron beam (also called a probe) is de-magnified by a series of electromagnetic lenses – condenser lens and objective lens.

The condenser lens is first in line and, based on the level of its excitation, changes its focal length. According to [2], the more current passes through the lens, the smaller its focal length becomes and vice versa. This is important, because between the condenser lens and objective lens, there is an objective aperture which limits how much of the electron beam is let through to the objective lens. Therefore, when the lens is excited more, by the time the probe reaches the aperture it gets wider and a smaller part of it passes through the aperture resulting in a smaller probe current and vice versa.

The objective lens is the most important part of the microscope regarding its resolution. It modifies the final size of the probe in its focal plane (also called a spot size), which is influenced by different aberrations of the objective – mainly spherical and chromatic. Astigmatism is also being taken seriously and it can be corrected by additional electromagnetic lenses called stigmators. Spot size is the determining factor in the final lateral resolution of the microscope, by definition. The possible resolution of an SEM is of the order of 1-10 nm, corresponding to an electron probe current of 10⁻⁹-10⁻¹² A [3].

A simplified construction of an SEM, including the display unit and the detector (discussed in part 1.1.2), can be seen in Fig. 1.1. The scanning coil is used for moving the probe across the sample in a raster scanning fashion (an x-direction line scan followed by a jump in the y-direction in order to scan the next line etc.). This is where the SEM got its name.

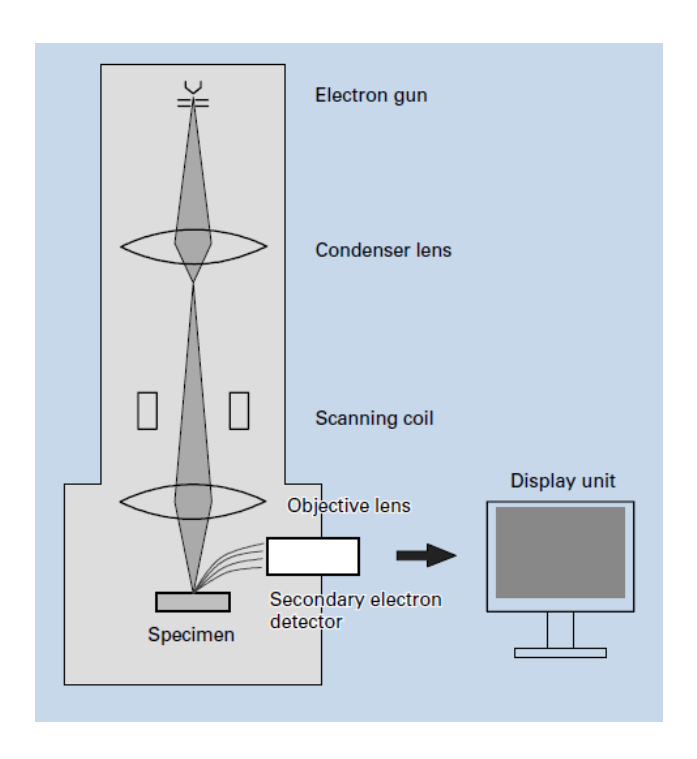


Fig. 1.1: Schematic of an SEM. From [2].

1.1.2 SEM imaging

The basic principle of SEM imaging is that the electron probe scanning of the surface of the sample is simultaneous with the image being created in the display unit (formerly cathode-ray tube (CRT), nowadays liquid crystal display (LCD)). The computer therefore records the current point being scanned by the probe and modulates the brightness of the corresponding pixel on the display according to the signal it receives from the detector [4]. An SEM image can have various forms depending on the type of interaction of electrons with the sample we focus on and detect.

There are two main types of atomic interaction an electron undergoes when it enters the sample – elastic and inelastic scattering. Elastic scattering is due to the electrostatic interaction with atomic nuclei and causes the electron to change its direction significantly while keeping its kinetic energy almost intact. Inelastic scattering is caused by an interaction with atomic electrons. It involves smaller deflection angles but reduces the kinetic energy of the incoming electron until it is absorbed by the material. The maximal depth an electron travels inside a material is called penetration depth. The volume of sample containing most of the scattered electrons is called the interaction volume. Both of these quantities depend on the energy of the incoming (primary) electrons, the density and the atomic number of the sample atoms. Increasing the energy of the primary electrons causes them to penetrate deeper, while increasing the density and/or atomic number of the sample atoms lowers the penetration depth, which is of the order of 10 nm -10 μ m [3, 4].

The lost energy of the penetrating electron due to inelastic scattering is gained by the interacting atomic electron. If it is a valence electron, it can gain more energy than is its work function and thus start moving through the sample as a secondary electron (SE)[4]. Its energy is relatively small, usually units of eV, by convention the cut-off energy is 50 eV [3]. Statistically only SE created in

a small depth below the surface (< 2 nm) called the escape depth actually escape from the sample, as the others interact inelastically with the sample themselves and lose the energy needed to escape [4]. We, therefore, receive mainly topographical information from them.

The electrons scattered elastically by an angle bigger than 90° are called backscattered electrons (BSE). This can happen by a single interaction or multiple ones adding up to more than 90°.BSE can have a wide range of energies from $E_{\rm BSE}=50~{\rm eV}$ up to almost the energy equal to that of the primary electron as can be seen in Fig. 1.2 b). Because during an elastic scattering their energy does not change much, BSE can escape from up to half the penetration depth (Fig. 1.2 a)). According to [4], the backscattering coefficient η (the number of escaped BSE divided by the number of incident electrons) increases with atomic number Z, so in BSE images we can mainly see material contrast (or topographic contrast, if we use only low-loss electrons, which have a small escape depth). To detect BSE, a detector covering a large solid angle must be used, because, due to their high energy, BSE travel in straight lines unaffected by electrostatic fields. Usually, a metal ring detector located between the sample and the objective is used.

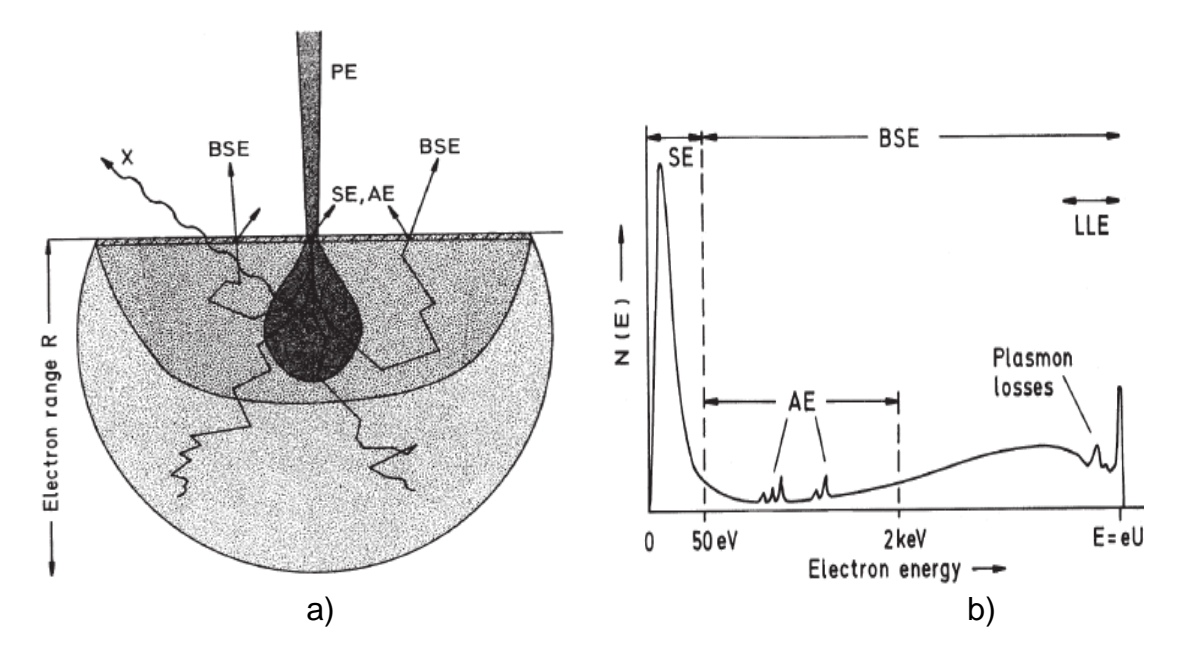


Fig. 1.2: a) Volume from which we gain information from secondary electrons (SE), backscattered electrons (BSE), Auger electrons (AE) and X-rays (X) for primary electrons (PE) incident perpendicular to the surface. b) Schematic energy spectrum of escaped electrons consisting of secondary electrons (SE) with energies $E_{\rm SE} \leq 50~{\rm eV}$, backscattered electrons with energies $E_{\rm BSE} > 50~{\rm eV}$ up to the energy of primary electrons E = eU (low-loss electrons – LLE) and in between peaks of Auger electrons (AE). Both are from [3].

To detect SE, an Everhart-Thornley detector (Fig. 1.3) mounted on the side of the chamber is most frequently used. Escaped SE are first accelerated towards a positively biased grid. The electrons which passed through are then accelerated further towards a scintillator biased positively by a voltage of several thousand volts. The scintillator can be a layer of phosphor on a glass rod. It has a property of cathodoluminescence, which means it emits photons when struck by charged particles. The photons are then guided by internal reflection to

a photomultiplier tube (PMT) located outside the vacuum. The PMT contains a photocathode, which is made from a material with a low work function. Photons hitting the photocathode can give its electrons enough energy to escape into the vacuum of the PMT. In the PMT, the electrons are then accelerated towards a first of a series of electrodes called dynodes, each biased positively by about a 100 V more than the previous one. The dynodes are coated with a material generating at least 2 electrons for every electron incident on it. There are enough dynodes to generate a current measurable with an ammeter [4]. The brightness of the final image is modulated based on this current value.

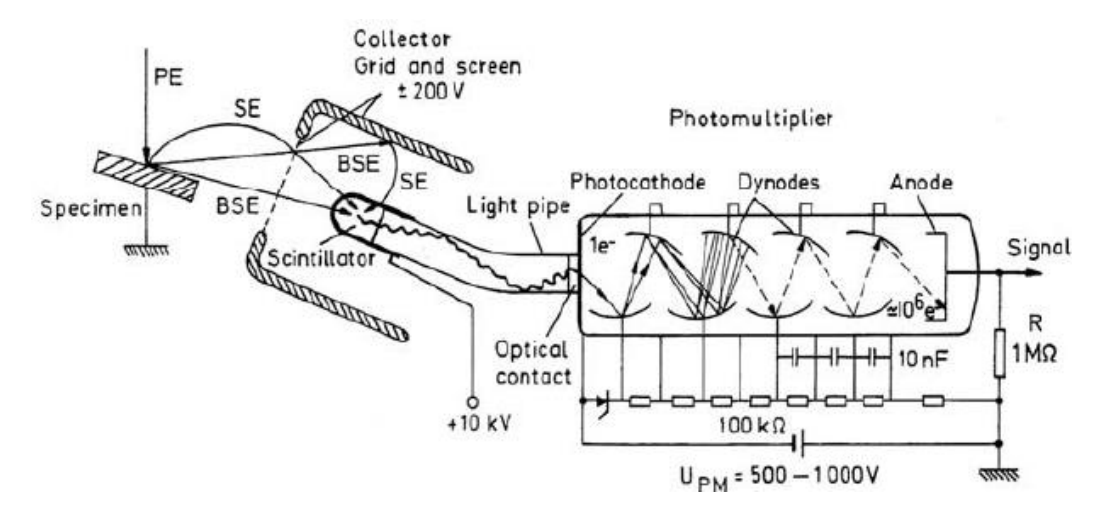


Fig. 1.3: A typical Everhart-Thornley detector. From [4].

There is a second type of detector used for SE called an in-lens detector. This detector is used in high-resolution SEMs, when the sample is so close to the objective that the SE are affected by its magnetic field. After escaping the sample, the electrons follow helical trajectories around the optical axis of the microscope towards a positively biased detector located above the objective lens. The images from such detector do not show effects caused by the difference of detector position as is the case with the Everhart-Thornley detector [4].

1.2 Atomic force microscope

Scanning probe microscopy (SPM) is an umbrella term for many techniques used to examine the surface topography or the local properties of the sample. The main part of these microscopes is a very sharp tip, ideally having a single atom at the end. Due to such a small tip these techniques can achieve a very good lateral resolution. For imaging, any kind of interaction of the tip with the sample surface can be utilized [5].

The first SPM was the scanning tunnelling microscope (STM), which uses tunnelling current through a vacuum between the tip and a conducting sample to record the topography of the surface with atomic resolution. This invention made in 1981 even resulted in The Nobel Prize in Physics in 1986 for its inventors G. Binnig and H. Rohrer [5].

The second innovative and nowadays widely used member of the SPM family capable of achieving atomic resolution was the atomic force microscope (AFM). It was developed in 1986 by G. Binnig, C. F. Quate and Ch. Gerber to improve on the STM's main weakness – not being able to investigate surfaces of insulators (although it works for conductors too). As is written in their original paper: "The atomic force microscope is a combination of the principles of the scanning tunneling microscope and the stylus profilometer." [6]

1.2.1 Basic working principle of AFM

The AFM can be used to acquire data either about topography or the local properties of the sample (electrical, magnetic, mechanical, etc.). It does this by recording the interactive force (or rather quantities proportional to the force) between the sample and the probe together with the currently scanned position of the sample.

The probe of an AFM consists of an elastic cantilever with a small tip attached to the free end. What we measure in the AFM is either the deflection or the change in oscillations of this cantilever due to the interactive force between the tip and the sample.

The interaction is actually very complex, but it can be qualitatively described by examining intermolecular forces e.g., the van der Waals forces between single atoms. The potential energy of two atoms separated by a distance r can be approximated by the Lennard-Jones potential U_{LJ} :

$$U_{\rm LJ}(r) = U_0 \left[\left(\frac{r_0}{r} \right)^{12} - 2 \cdot \left(\frac{r_0}{r} \right)^6 \right],\tag{1.2}$$

where U_0 is the minimum of the potential and r_0 is the distance between the atoms in this minimum. The graph of this potential is shown in Fig. 1.4. The physical interpretation of the equation is following: the first term in the square bracket represents the short-range repulsion of the electron clouds (Pauli exclusion principle). Conversely, the second term represents the long-range attraction due to the van der Waals force [5]. To get to the point, we can simplify the otherwise numerous interactions of all the atoms of the tip with all the atoms of the sample to a single most important one - one atom at the end of the tip interacting with one atom on the surface of the sample closest to this atom.

The force \vec{F} acting on the tip due to this potential can then be estimated as:

$$\vec{F} = -grad (U_{LJ}). \tag{1.3}$$

$$U_{LJ}$$

$$U_{0}$$

(1.3)

1.2.2 Contact mode

Depending on how the AFM acquires data for the image, we can distinguish two main modes of its operation - contact mode (quasi-static) and dynamic modes (including non-contact and semi-contact mode).

The principle of contact mode is similar to that of the stylus profilometry as was mentioned in the original paper [6]. In both of these techniques the probe consists of a cantilever carrying a tip physically touching the surface as it scans over it. Then, the deflection (proportional to the interaction force) of the cantilever is being recorded at every scanned point, while a feedback system keeps a constant setpoint - torque/force -chosen by the operator as shown in Fig. 1.5. From this data, the topology of the surface can be reconstructed [5,7]. The difference between the two is in the advance in technology and knowledge needed for them to function. "While stylus profilometry is an extension of human capabilities that have been known for ages and works by classical mechanics. AFM requires a detailed understanding of the physics of chemical bonding forces and the technological prowess to measure forces that are several orders of magnitude smaller than the forces acting in profilometry." [8] The main disadvantage of both techniques is that, because they are in contact with the sample, they can damage softer surfaces or the tip. Therefore, in contact AFM, a cantilever softer than the sample is used so as to be more sensitive and not plastically deform the sample [5].

The feedback system is an important part of the AFM for automatic control of the tip-surface distance when scanning over the surface of a sample. It keeps a certain quantity constant and observes the changes in another quantity to map the scanned area. In contact mode, usually the force (corresponding to some bend of the cantilever) is kept constant, and we observe deflections of the cantilever, as was described in the previous paragraph, eventually resulting in a 3D topography image. The deflection of the cantilever is most often measured by a laser and a photodiode. The photodiode is divided into four quadrants. At the beginning, the laser, reflecting off the top part of the cantilever, illuminates the middle of the photodiode - receiving the same photocurrent in every quadrant. As the cantilever is deflected, the spot on the photodiode moves accordingly and by simple addition and subtraction of the signals from different pairs of quadrants, the direction and magnitude of the deflection can be measured. The voltage, which is proportional to this change in photocurrent from its original value, is then processed through various amplifiers and compared with the set-point (set by the operator). This final value is then fed to a piezoelectric motor (scanner) which moves the sample in the z-direction in order to keep the distance between the tip and the surface constant (effectively, keeping the interaction force constant). All the voltages, corresponding to the movements of the scanner in the z-direction during scanning over the surface of the sample, are recorded and, together with the respective positions of the tip over the sample, an image of the surface's topography can be generated from them in a computer [5].

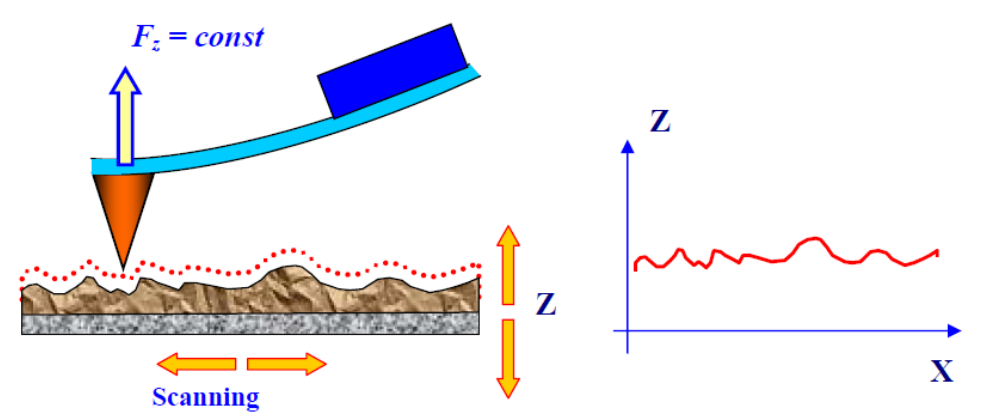


Fig. 1.5: Contact mode AFM working at constant force. From [5].

1.2.3 Dynamic modes

Dynamic modes help solve the main problem of contact mode – damaging the sample surface. In such modes, the cantilever is driven to oscillate (usually by a piezovibrator) with a certain frequency at some height over the sample. We can differentiate between non-contact mode and semi-contact (tapping) mode [5].

By solving the motion equation of a forced damped oscillator in a force gradient F_2 , we get the amplitude-frequency characteristic $A(\omega)$:

$$A(\omega) = \frac{u_0 \omega_0^2}{\sqrt{\left(\omega_0^2 - \omega^2 - \frac{F_z}{m}\right)^2 + \frac{\omega^2 \omega_0^2}{Q^2}}},$$
(1.4)

where u_0 is the amplitude of the driver's oscillations, ω is the driving frequency, ω_0 is the natural frequency of the cantilever and Q is the quality factor defined as

$$Q = \frac{\omega_0 m}{\gamma},\tag{1.5}$$

where m is the mass of the cantilever and γ is the damping coefficient. We also get the relationship for phase shift $\varphi(\omega)$ (the phase difference between the driver and the cantilever) as:

$$\varphi(\omega) = \arctan\left[\frac{\omega\omega_0}{\left(\omega_0^2 - \omega^2 - \frac{F_Z'}{m}\right)}\right]. \tag{1.6}$$

The resonance frequency $\omega_{\rm rf}$ in this system can be written as:

$$\omega_{\rm rf}^2 = \omega_0^2 \left(1 - \frac{1}{20^2} - \frac{F_z'}{k} \right), \tag{1.7}$$

where k is the stiffness of the cantilever. The difference between the frequency $\omega_{\rm rf}$ and ω_0 is called a frequency shift and together with the previous relationships (Eq. 1.4., 1.5. and 1.6.) is used in the feedback loop and thus obtaining signal for images in the dynamic modes of the AFM [5].

In non-contact mode (also called frequency modulation AFM: FM-AFM), the cantilever is driven at its resonance frequency maintaining the oscillation amplitude constant (set by the operator). As the cantilever is in the lower part of the oscillation, it gets into the force gradient of the tip-sample interaction. This causes a frequency shift (described by Eq. 1.7), which can be detected and used in the feedback loop to keep the amplitude constant and as a signal for the AFM image [9, 10]. There is also a corresponding phase shift, which is also proportional to the force gradient and can be used to generate a phase contrast AFM image [5].

In tapping mode (also called amplitude modulation AFM: AM-AFM), the cantilever is driven with a fixed frequency near its resonance. When approaching the sample, the resonance frequency of the cantilever shifts due to the force gradient (change in the effective stiffness of the cantilever). This also results in the change of the oscillation amplitude, because the driving frequency does not change while the amplitude-frequency characteristic moves. By detecting these changes in the amplitude, an AFM image can be created from this signal [9, 10]. Considering the energy exchange through one oscillation, we can arrive at the following conclusion: "The cantilever oscillations phase shift in "semi-contact mode" is determined by the amount of dissipative tip-sample interaction." [5] This can be also used to create a phase contrast AFM image.

1.3 Heterogeneous catalytic CO oxidation

Usually, a chemical reaction operated at constant external parameters forms the products at a steady rate. For some reactions, though, there exist conditions, under which the reaction rate oscillates periodically or aperiodically in time. The most known example is the Belousov-Zhabotinsky (BZ) reaction in a stirred homogeneous solution, in which the rate oscillations can be clearly seen by observing the colour changes of the solution in time. Similar rate oscillations have also been found in other reactions e.g., heterogeneous catalytic reactions at gas-solid interface. These reactions exist far from thermodynamic equilibrium and are guided by nonlinear dynamics. Such systems give rise to various phenomena, like rate oscillations, spatiotemporal patterns and deterministic chaos. This chapter will focus on the description of a conceptually simple example - heterogeneous catalytic CO oxidation, which can act as a stepping stone to explaining the phenomena occurring in more complex reactions and situations [11, 12].

1.3.1 Reaction mechanism

This system can be simply described as a reaction of carbon monoxide (CO) and oxygen (O_2) , resulting in the creation of carbon dioxide (CO_2) , on the surface of platinum (Pt), which acts as a catalyst (heterogeneous simply means that the reactants and the catalyst have different phases, in our case – reactants are gases, and the catalyst is a solid). Its mechanism can be described by a Langmuir-Hinshelwood (LH) scheme expressed by the following equations:

$$CO + * \rightleftarrows CO_{ad}, \tag{1.8}$$

$$O_2 + 2 * \rightarrow O_{ad},$$
 (1.9)

$$O_{ad} + CO_{ad} \rightarrow CO_2 + 2 *,$$
 (1.10)

where the bottom index ad denotes adsorbed reactants and \ast represents a free adsorption site. The actual mechanism is a bit more complicated. Both CO and O2 compete to be adsorbed, but there is a big difference. O2 needs to first dissociate into two atoms, which requires a large unoccupied area on the platinum surface, creating an open adlayer which still allows CO to adsorb. The O2 molecule also needs enough energy to dissociate into two O atoms, which requires a higher temperature of the sample. On the other hand, CO needs only a single free surface atom for adsorption, forming a dense adlayer, completely preventing O2 from adsorbing and reacting. The platinum surface, which is covered like this, has a lowered catalytic activity and is so-called poisoned by carbon monoxide. This can be reversed only by heating it to a higher temperature - desorbing the CO from the catalyst surface. CO_2 is then created by the recombination of CO_{ad} with O_{ad} and is released into the gas phase. The reaction rate R can be simply given as:

$$R = \frac{dp_{CO_2}}{dt} = k \cdot u_1 \cdot u_2,\tag{1.11}$$

where k is the rate constant for the surface recombination of CO and O, and u_1 , u_2 are the surface concentrations (coverages) of adsorbed CO and O respectively, which can be further obtained from integrating a particularized set of partial differential equations known as reaction-diffusion equations:

$$\frac{\partial u_i}{\partial t} = F_i(\lambda, \boldsymbol{u}) + D_i \frac{\partial^2 u_i}{\partial x^2},\tag{1.12}$$

where \boldsymbol{u} is the vector of concentrations of the individual components, λ represents parameters like temperature, pressure or the sticking coefficients of oxygen - s_{O_2} , and of carbon monoxide - s_{CO} . The term F_1 represents the kinetics of component i, while diffusion is contained in the second term with D_1 being the diffusion coefficient. Often, we can assume spatial homogeneity, neglecting the second term on the right and getting a set of ordinary differential equations instead [11, 12].

1.3.2 Reaction rate oscillations

This subchapter is heavily inspired by [11], so if there is no citation given, assume the source is this paper.

Firstly, the aforementioned difference in absorption between CO and O₂results in a bistability of the system. We can distinguish between two branches: a high-rate branch when the partial pressure of CO, $p_{\rm CO}$ is low, for which the reaction rate increases linearly with increasing $p_{\rm CO}$ (so-called CO adsorption limited reaction), and a low-rate branch for high $p_{\rm CO}$, in which the reaction rate decreases with increasing $p_{\rm CO}$ due to the poisoning of the surface.

Secondly, for certain combination of control parameters (temperature and partial pressures of CO and O_2), oscillations of the production rate of CO_2 are observed. This is explained by the reconstruction model, which will be described further.

Concerning the Pt(111) orientation, this surface is the only one stable in its bulklike state due to the atoms being densely packed. During experiments, it did not display oscillations, but it was possible to observe the bistability of the reaction.

The Pt(100) and Pt(110) 1 × 1 surfaces corresponding to the bulk arrangement are more open and so more structurally unstable. The Pt(100) surface reconstructs into a hex structure, while the Pt(110) surface reconstructs into a 1 × 2 missing row type as can be seen in Fig. 1.6. The reconstructions can be explained thermodynamically – the reconstructed surface has a lower surface energy compared to the original 1 × 1 surface. However, the reconstruction can be lifted if the increase in adsorption energy of an adsorbate e.g., CO, is bigger than the energy needed for reconstruction. Some adsorbates can have different sticking coefficients depending on the structure of the surface. For Pt(100) the oxygen sticking coefficients differ extremely between the two phases:

 $s_{0_2}^{1\times 1}\approx 0.3$ and $s_{0_2}^{hex}\approx 10^{-4}-10^{-3}$. For Pt(110) the difference is much smaller: $s_{0_2}^{1\times 1}\approx 0.6$ and $s_{0_2}^{1\times 2}\approx 0.3-0.4$.

Rate oscillations are connected to conditions, for which the limiting factor is oxygen adsorption. The conditions enabling oscillations can be seen in Fig. 1.7. The rate oscillation can have the following course. Assume a clean Pt surface, which reconstructed to its more stable phase. When exposed to CO, the surface reconstruction is lifted to 1 × 1 phase after reaching a critical coverage of $\theta_{\rm CO,crit}\approx 0.2$. The oxygen sticking coefficient is higher for this phase and so the adsorption of oxygen increases resulting in a higher catalytic activity, producing more CO₂. This continues until the coverage of CO decreases below the critical value $\theta_{\rm CO,crit}$ and the reconstruction of the surface is again more thermodynamically preferred. However, the reconstructed surface has a lower $s_{\rm O_2}$ and so again, the CO coverage can increase. This takes us back to the original point and by this mechanism being repeated, rate oscillations can be observed.

Even higher index planes, such as Pt(210), can exhibit rate oscillations, but there is a delay of about 10-30 minutes after exposing it to reaction conditions. That is because this surface itself does not reconstruct, but a different phenomenon is responsible – faceting. Faceting means reordering of surface atoms forming steps and terraces, which can have different orientations. The Pt(210) surface facets into (110) and (310) orientations. Concerning Pt(110), the existence of oscillations was already described before. Although, there is a small difference – the possible temperature is restricted to $T < 500 \, \text{K}$ due to the atoms being more mobile, preventing the facets from occurring.

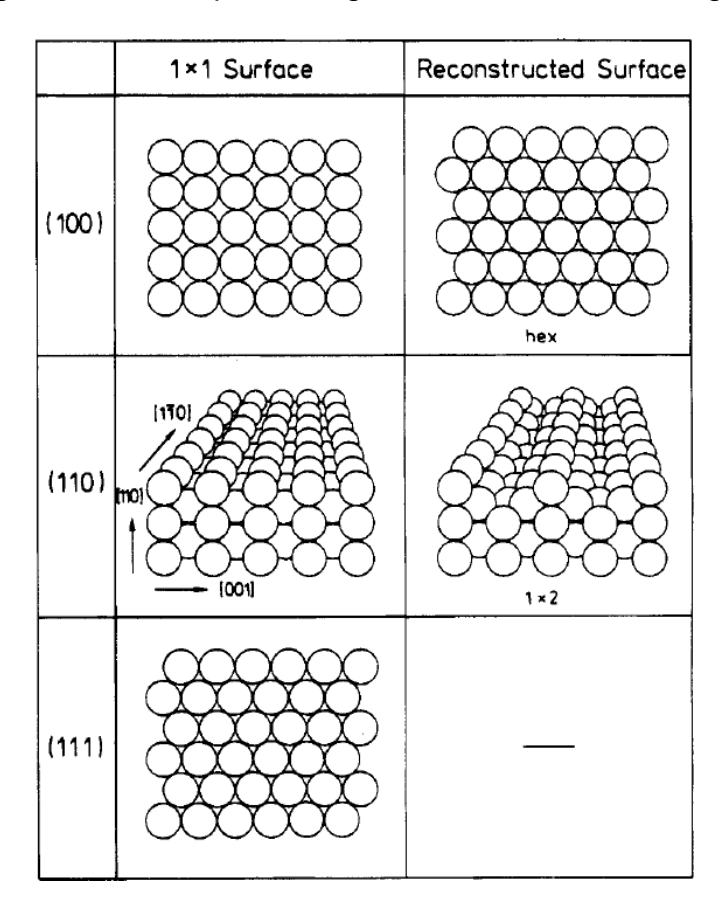


Fig. 1.6: Reconstruction of surfaces for the low-index planes of Pt. From [11].

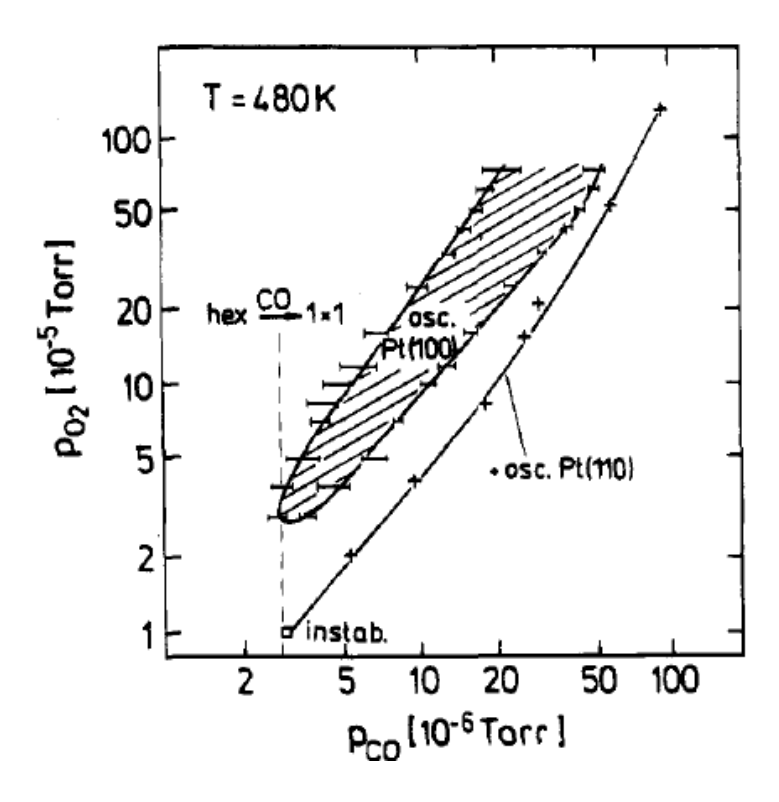


Fig. 1.7: Possible partial pressures of adsorbates for the occurrence of rate oscillations at T = 480 K. The dashed line represents the minimum p_{CO} needed for lifting the hex reconstruction on Pt(100). From [11].

1.3.3 Spatiotemporal patterns

Many oscillatory systems also display forming of spatiotemporal patterns. Their regularity depend mainly on how well the surface parts are coupled (different types will be described in the next subchapter). It is also connected to the range of the possible parameters shown in Fig. 1.7. E.g. for Pt(100), for a given temperature and partial pressure of O₂, the partial pressure of CO can be very different to still produce oscillations, which results in irregular oscillations and thus irregular spatiotemporal patterns [11].

Concerning Pt(110), the landscape of possible patterns is much larger. Many of these patterns are present also in other types of reactions like homogeneous reactions in solution, such as the well-known and studied Belousov-Zhabotinsky reaction. In this reaction, the concentration changes, showing as colour changes, can be seen simply by eye. For our reaction, the difference is in the techniques needed to observe these microscopic patterns on the surface. The patterns vary based on the combination of the control parameters. Some of them are target patterns – circular chemical waves moving out from a point on the surface, where a surface defect is present. When two such waves intersect, they destroy each other, creating sharp edges. These waves can be accompanied by a long-range coupled temporal oscillation of the background between a CO and O covered surface. Under different parameters, growing spiral waves can be seen. These are present in many reaction-diffusion systems and so are well studied. They are usually pinned to macroscopic defects, the size of which decides the wavelength of the spiral. However, they can be unpinned by changing the control parameters. Both target patterns and spirals are elliptical, expanding at different velocities in different directions which can be described by the anisotropy of the diffusion coefficient. Constant shape pulses moving uniformly across the surface were also observed. Sometimes, the interaction of two pulses does not result in their destruction, but they continue further unaltered. At higher temperatures, stationary waves replaced propagating waves. During these waves, the macroscopic features changed simultaneously over the entire surface. By varying a single parameter, the patterns get increasingly more irregular, eventually resulting in chemical turbulence [11, 13].

1.3.4 Spatiotemporal self-organization

In order to observe such regular patterns (corresponding to a regular change of a macroscopic quantity such as the rate of production of CO₂), as described in part 1.3.3, a certain synchronization or coupling mechanism has to be present. Otherwise, the contributions of the individual local oscillations would result in an averaged steady reaction rate [11].

According to [12], there are three main coupling principles:

1) Heat conductance.

This is the main coupling principle of non-isothermal systems at atmospheric pressure, where the local temperature differences due to the exothermicity or endothermicity of the reaction can reach up to 100 K. The heat from these reactions moves through the sample to synchronize it. In low-pressure systems, the temperature oscillations are of the order of 0.05 K, so this effect can be neglected.

2) Gas phase coupling

The changes in reaction rate also bring about variations in the partial pressures of the reactants. Under low pressure conditions, these local changes in partial pressures can reach other parts of the sample almost instantly (in < 10^{-3} s, much quicker than the oscillation period). In CO oxidation, the change in $p_{\rm CO}$ can be around 1 %. Experiments with forced oscillations showed that Pt(110) responded to periodic modulations of $p_{\rm CO}$ < 1% (this is due to the small range of possible parameters causing oscillatory behaviour as can be seen in Fig. 1.7). With good approximation, this can be considered as the coupling principle responsible for oscillations in Pt(110) at low pressures.

3) Surface diffusion coupling

This process is associated with oscillations on Pt(100), for which the interval of possible parameters is much larger (Fig. 1.7), so the changes in $p_{\rm CO}$, responsible for gas phase coupling, are not enough to significantly affect the reaction. Experiments showed that a change in $p_{\rm CO} > 5\,\%$ is needed for oscillations. Instead, local differences in concentration of adsorbates cause surface diffusion, resulting in chemical waves.

2 Experimental part

2.1 Apparatus and sample

This chapter will describe the sample and all the apparatus used during the experimental part of this thesis.

2.1.1 Sample preparation

The catalyst sample used was a platinum wire with a diameter of 0.2 mm. A piece around 5 cm long was cut and shaped into a V-shape to minimize thermal drift due to heating while observing it in the SEM. It was consequently flattened with a press (which also made one of its sides shiny as seen in Fig. 2.1) to increase its surface area in order to be able to see more grains and thus find more active grains, which are grains capable of producing spatiotemporal patterns, too. This sample was then attached to a sample holder as seen in Fig. 2.1 a). The sample holder was then inserted into the airlock and transported through the loadlock into the main chamber of the UHV-SEM (seen in Fig. 2.2) for heating and observation of the sample. After an experiment was finished for the day, it could be stored inside the carousel part of the microscope, protecting it from the exposure to the atmosphere. For the HV-SEM experiments, the sample holder was, simply, manually inserted inside the microscope.

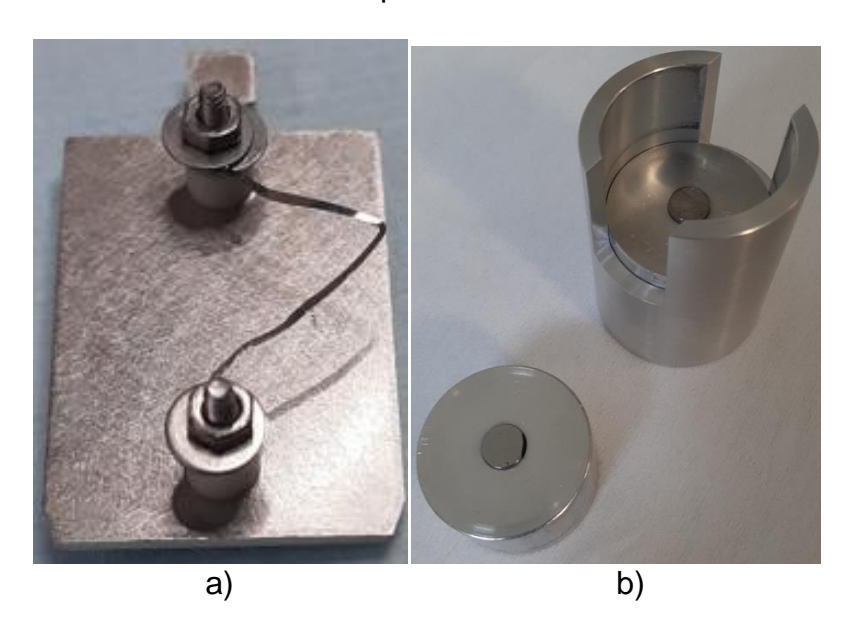


Fig. 2.1: a) Pt wire sample used for the oxidation of CO. Its ends are wound around bolts, through which it can be heated by resistive heating. b) Tungsten press used to flatten and shine the wire into the sample seen in a).

2.1.2 Ultra-high vacuum SEM

The microscope used for the first part of the experiments can be seen in Fig. 2.2 and schematically in Fig. 2.3. It is an ultra-high vacuum SEM (UHV-SEM) from TESCAN.

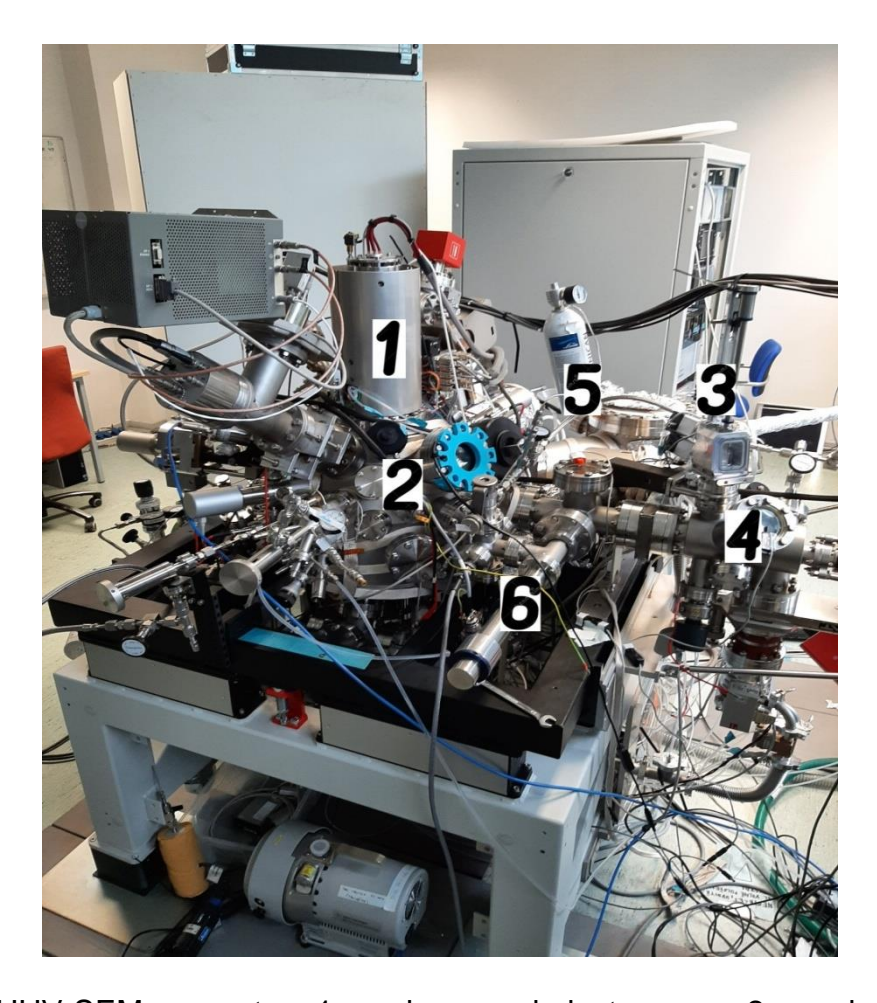


Fig. 2.2: UHV-SEM apparatus. 1- column and electron gun, 2- main chamber, 3- airlock, 4- loadlock, 5- gas feeding system, 6- carousel.

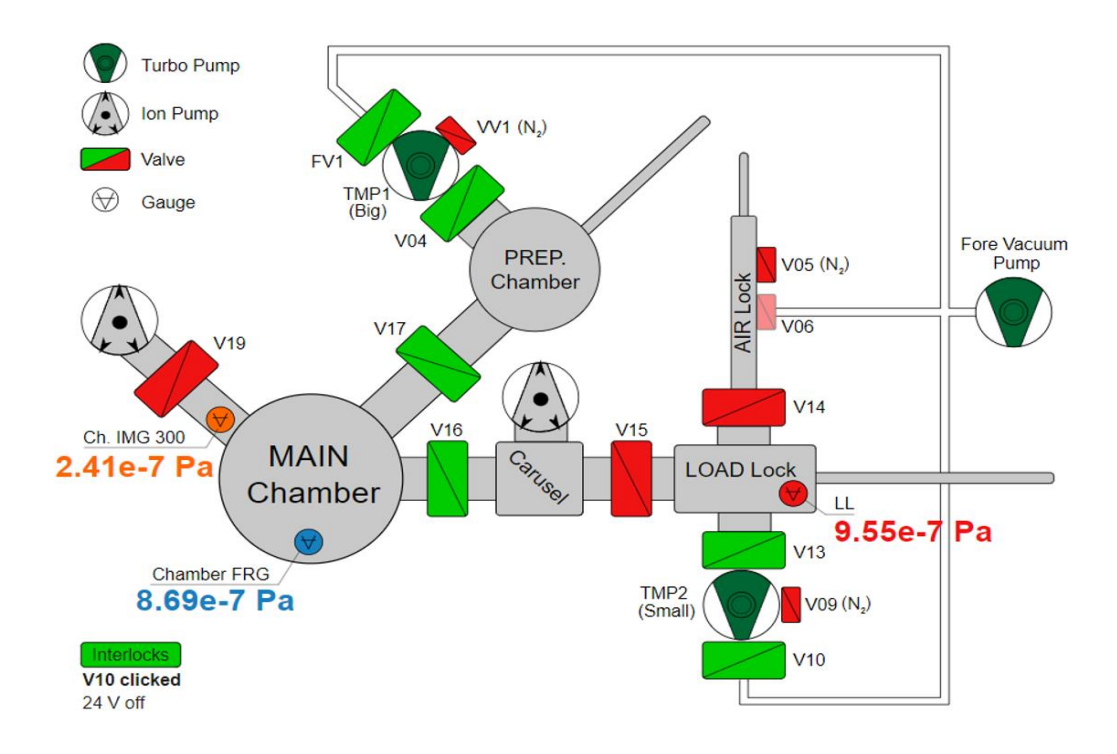


Fig. 2.3: Schematic diagram of the UHV-SEM in Fig. 2.2.

The UHV-SEM was mainly pumped by two turbomolecular pumps. The system was pre-pumped by a rotary pump. The entirety of the first part of the experiments was done exclusively in the main chamber (sample cleaning and reaction observation). The pressure in the main chamber was measured by two gauges as seen in Fig. 2.3. The green valves in this figure are opened and this is how it was set up during the experiments. The gases injected into the microscope flowed into the main chamber and was pumped out through the preparatory chamber by a big turbomolecular pump, effectively creating a flow reactor. The temperature of the sample was measured from outside by a pyrometer with a range of $190 \, ^{\circ}\text{C} - 1 \, 000 \, ^{\circ}\text{C}$.

2.1.3 High vacuum SEM + AFM

The second part of our experiments was carried out in a high vacuum SEM (HV-SEM) from Thermo Fisher Scientific (seen in Fig. 2.4). The AFM used (Fig. 2.5) was produced as a part of a student collaboration on the Institute of Physical Engineering at Brno University of Technology (IPE at BUT). The lowest pressure achievable in this setup was around $p=5\cdot 10^{-4}\,\mathrm{Pa}$ and the maximal operation pressure of the microscope is $p=3.30\cdot 10^{-2}\,\mathrm{Pa}$.

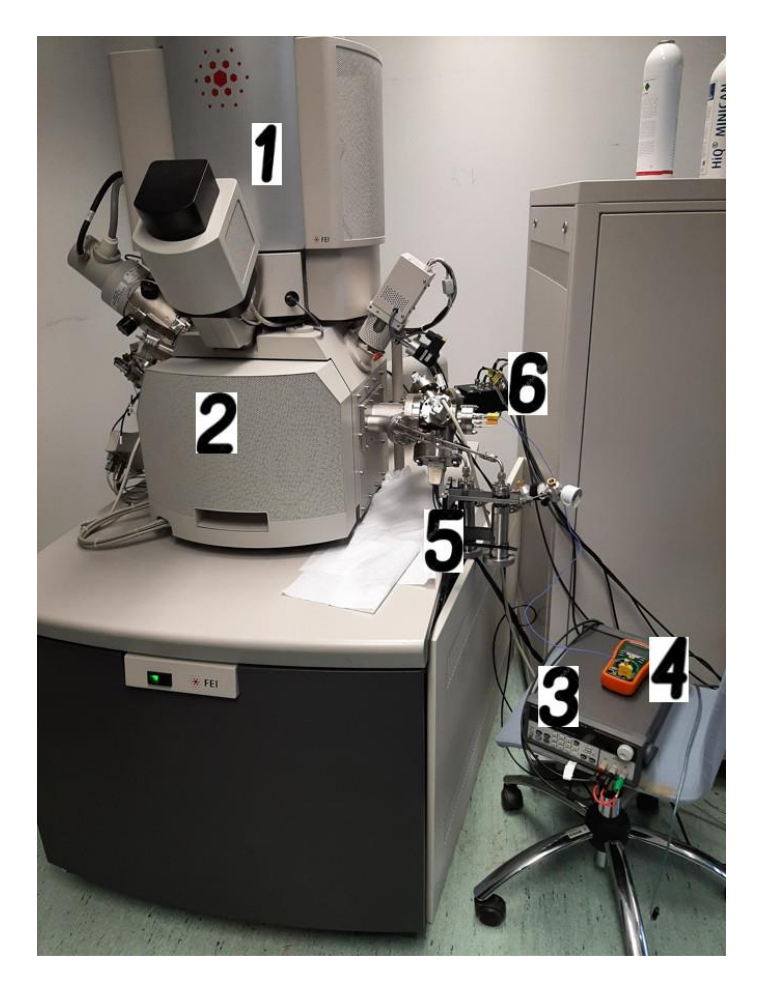


Fig. 2.4: HV-SEM apparatus with an AFM inside. 1 –column and electron gun, 2 – chamber, 3 – power supply for heating of the sample, 4 - multimeter for measuring the temperature of the AFM scanner by a chromel-alumel thermocouple, 5 – gas feeding system, 6 – AFM connectors.

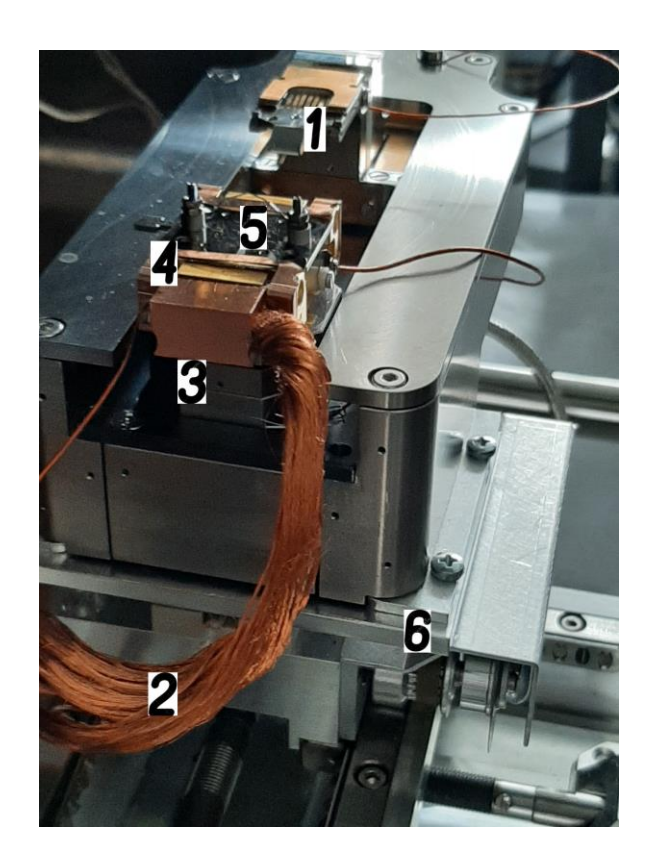


Fig. 2.5: AFM apparatus installed inside the HV-SEM chamber. 1 – scanning head with a probe, 2 – copper wires for redirecting heat from the sample holder to protect the AFM scanner, 3 – AFM scanner, 4 – sample holder needed for AFM, 5 – the original sample holder used in UHV-SEM, 6 – AFM holder needed to attach the AFM to the HV-SEM sample manipulator.

2.2 UHV-SEM reaction

The first part of the experiments concerns the CO oxidation on Pt observed in a UHV-SEM, which can achieve minimum pressures of the order of $p = 10^{-7}$ Pa and has a maximal operation pressure of $p = 1 \cdot 10^{-2} \, \mathrm{Pa}$. The general procedure, after the sample was already placed in the main chamber, started with cleaning of the sample in oxygen atmosphere of around $p_{0_2} = 2 \cdot 10^{-3} \, \mathrm{Pa}$. The sample was simultaneously heated resistively by an electrical current $I = 2.60 \,\mathrm{A}$ flowing through it, corresponding to temperatures of above $T = 1000 \,^{\circ}C$ (the exact temperature could not be known, because the pyrometer used to measure it had a range of $T \in <190$ °C; 1000 °C >. Such temperature was still below the melting point of Pt, which is $T_{\rm m}=1768\,{}^{\circ}{\rm C}$. This was done for about 60 min, or until no more contamination was seen on the SEM image. Then, the current was turned off and the oxygen influx was stopped completely until pressure dropped to its original value of the order of $p = 10^{-7}$ Pa. Such base pressure secures the cleanliness of the sample for a long time (several hours) and, on top of that, makes it so that basically only CO and O2 have an impact on what happens on the Pt sample surface during the reaction.

After this cleaning procedure, the finding of the reaction conditions could be started. At first, the current was set to a value of around I = 0.70 A, to prevent CO poisoning. Secondly, the partial pressure of CO was set to some value, which

would not be changed during an experiment e.g., around $p_{\rm CO}=2\cdot 10^{-4}\,{\rm Pa}$. Assuming that the ratio of the partial pressures of the gases to be the important thing and not the absolute value of either for oscillations to happen at all. The absolute values have more to do with what type of reaction waves would occur as hinted at in [13]. The partial pressure of O2 was then set so that their ratio started at around $\frac{p_{0_2}}{p_{co}} = 4$. The current (correspondingly, also temperature) was then increased periodically up to about $I = 1.30 \, \text{A}$. Keeping in mind that the sample is polycrystalline, and that the reaction occurs only on select grain orientations as described in 1.3.2, a wide field of imaging was used to spot any active grains. If no chemical wave passed over any grain, resulting in a change of contrast, the ratio of the partial pressures was increased by increasing the oxygen partial pressure and the process was repeated. If there was a change in contrast, the current was modified to find its critical value corresponding to the reaction wave occurring. When the correct parameters were, finally, found, the oscillations were self-sustained and were active for some time (of the order of 30 minutes). Then, the oscillations could be prolonged by changing an external parameter, but eventually, the surface was entirely covered with a single adsorbate, and it was not possible to change the contrast by any means. This can, perhaps, be explained by the presence of carbon contamination on the sample surface, which was created by the decomposition of the adsorbed molecules of CO into carbon by the electron beam of the microscope. This contamination could only be disposed of by heating the sample to a very high temperature. After this, the temperature can be decreased, and the oscillations can be started up again.

The concrete experiment performed can be seen in Fig. 2.6. This experiment started by heating the wire by electrical current to around $I = 1.00 \,\mathrm{A}$, because from previous experiments it was clear that the reaction occurs at currents lower than this value. Then, the partial pressure of CO was set to $p_{\rm CO}=2\cdot 10^{-4}~{
m Pa}$, which was unchanged during the experiment. The ratio of partial pressures started at $\frac{p_{\rm O_2}}{p_{\rm CO}}=4$. The current was slowly lowered to $I = 0.90 \,\mathrm{A}$, when a chemical wave of CO was observed on the left grain as can be seen in a). Although this wave was dark, which is commonly attributed to oxygen, it was identified as CO, because it started moving while lowering the temperature of the sample. As was described in part 1.3.1, oxygen needs a higher temperature of the sample, so it was assumed, that all the grains were oxygen covered at the starting temperature. The movement of this wave could be controlled by increasing and/or decreasing the current, which agreed with this assumption. The ratio of partial pressures was then increased to $\frac{p_{0_2}}{p_{co}} = 5.5$ in an attempt to balance the coverage on this grain, which could then result in oscillations by changing the temperature. The current was decreased further up until $I = 0.82 \,\mathrm{A}$, when the first change was observed on the active grain on the bottom of Fig. 2.6. Then, all the control parameters were kept constant and self-sustaining spatiotemporal patterns could be seen on the active grain. In a)-c), the start of the competition between the two adsorbates can be seen. These waves then evolve into spirals in d)-i), which are slowly getting more and more narrow. After the spirals faded out, the p_{O_2} was a bit increased along with the current, which resulted in the patterns seen in j)-k), but, eventually,

the surface was not responding to any change of parameters - I) and needed to be heated up to about $T > 1\,000\,^{\circ}\text{C}$ in order to get clean and reactive again.

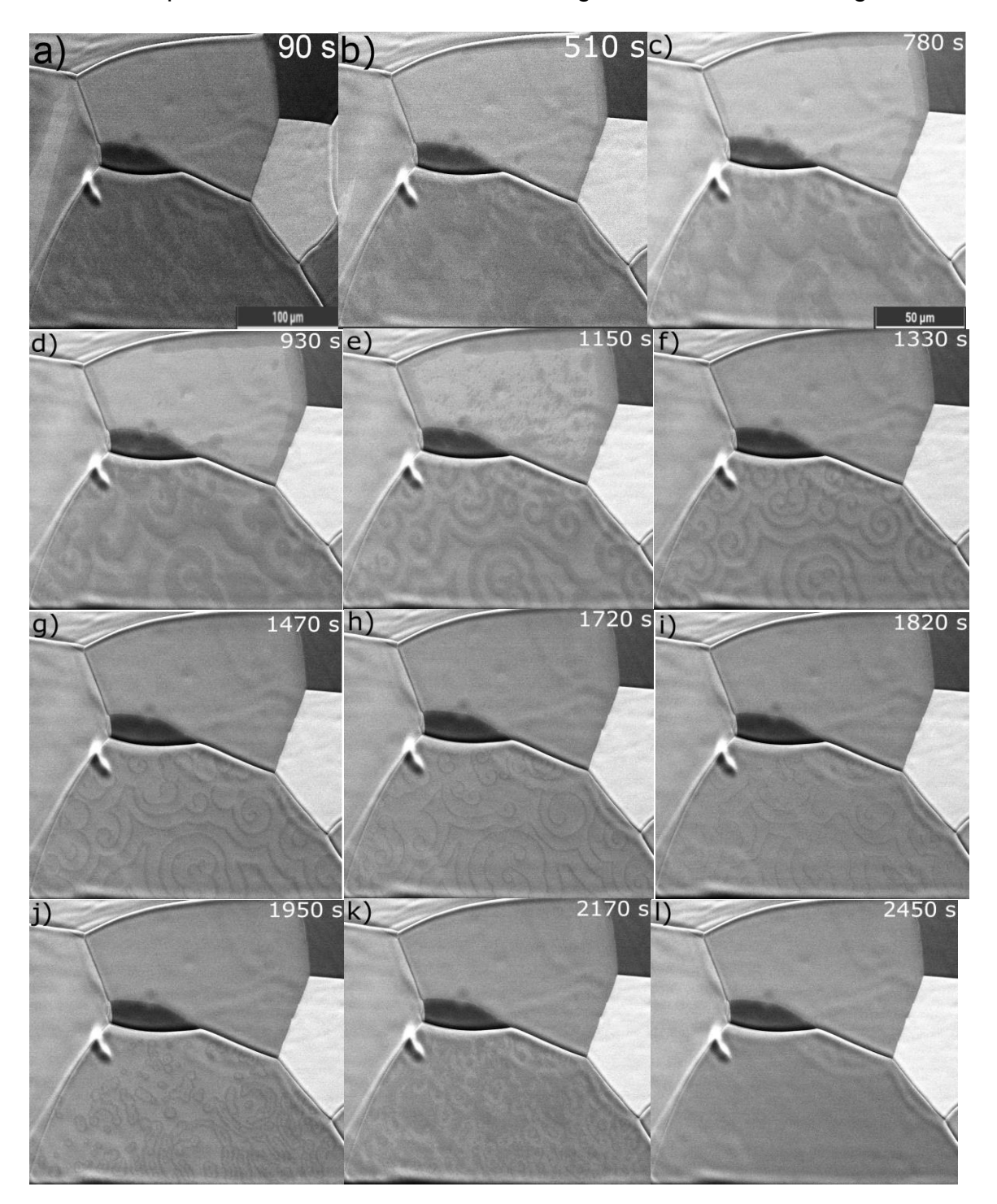


Fig. 2.6: Temporal progression of spatiotemporal patterns as seen in UHV-SEM. Control parameters since reaction started: $T=210\,^{\circ}\mathrm{C}$, $p_{\mathrm{CO}}=2\cdot10^{-4}\,\mathrm{Pa}$, $p_{\mathrm{O}_2}=1.1\cdot10^{-3}\,\mathrm{Pa}$. Dark areas are oxygen covered, bright areas are CO covered (this is true for our active grain at the bottom, for other grains, such as on the top and on the left of it, it may differ). The time $t=0\,\mathrm{s}$ corresponds to the first observable change on the active grain on the bottom.

2.3 HV-SEM reaction + AFM

The second part of the experiments (described in part 2.3.1) was done in the HV-SEM set up for our reaction, which consisted of installing a gas feeding system to the microscope, as seen in Fig. 2.4. Additionally, a sample holder for our original sample holder had to be made, to be able to insert the sample into this microscope, and which enabled the heating of our sample, and is seen in Fig. 2.5. Later, we were supposed to attempt a correlative probe and electron microscopy (CPEM) measurement of the reaction waves by using the AFM installed in the chamber of the microscope as seen in Fig. 2.5. The progress done and problems faced using the AFM is described in part 2.3.2.

2.3.1 HV-SEM reaction

The sample used for this reaction was the same as that mentioned in the previous part. Therefore, it had to be exposed to the atmosphere during the transport between the two microscopes. Even though it could be cleaned in the HV-SEM, it was not ideal to do for multiple reasons: the absence of a dedicated stage for heating, the lack of a pyrometer (not helpful at very high temperatures but could be of help in detecting unexpected circumstances during heating), and mainly the objective's sensitivity to heat, because it wasn't shielded from the heat yet. This is why the cleaning of the sample was first done in the UHV-SEM and then the sample was quickly moved to the other microscope.

There was something additional occurring during these experiments compared to the UHV-SEM measurements, as will be described further. We observed what was first thought of as a creation of particles on the sample surface, after setting up reaction conditions, with both CO and O_2 present, and heating the sample to a high temperature (corresponding to a current $I > 1.2 \, \text{A}$) as seen in Fig. 2.7. Later, we rather thought of it as a cleaning of some type – desorption of contamination, even though we were not exactly sure what it was. It always preceded the occurrence of reaction waves. We can see in Fig. 2.7 a)-c), the growing of the desorption areas. From c) to d), the temperature was lowered, and we can see no changes happened between the two images. In e), we can notice that it ignores grain boundaries, so it has nothing to do with reaction waves, which are grain dependent. In f), almost the whole field of view is cleaned, and this would happen over the entire sample in some time. After the desorption areas reached everywhere, the reaction could be started by changing the temperature, as has been described in part 2.2.

Concerning the observation of the actual reaction, it needs to be mentioned that during the experiment in Fig. 2.8, we used two different detectors, creating two images. We utilized a different detector for the analysis than the one used in Fig. 2.7, because we observed the reaction waves on the other side of the sample, which affected the quality of the image from the original detector, due do the directional effect of SEM detectors. However, this new detector had a different contrast to the one we are used to (dark – oxygen, bright – CO). This was tested by modulating the temperature of the sample and has no effect on the analysis of the measurement, other than that the contrast of the two adsorbates is swapped in the images.

The reaction we observed in the HV-SEM can be seen in Fig. 2.8. Again, for clarification, CO is dark, and oxygen is bright in these images. The images

form pairs, where in the first image we see a surface mainly covered with oxygen and in the second one we see that several seconds (~20 s) later, a reaction wave of CO has passed over the grain from the boundary resulting in the surface being somewhat evenly covered with both adsorbates for a while. These phenomena kept repeating with either of two things happening in between: a) the surface getting gradually more covered with oxygen for about 90 s or b) even more unpredictable patterns occurring on the surface with smaller, more frequent waves of CO appearing and disappearing again. This reaction was, therefore, much more unpredictable (not chaotic) than the one done in the UHV-SEM, even though the same spot was observed. This may have to do with the much (about fifteen times) larger absolute values of the partial pressures of the reactants, even though their ratio was similar to the previous experiment, but we used such pressures to minimize the effect of the residual gases and to utilize the higher operational pressure of the microscope. Also, a very high sensitivity of the reaction to temperature was observed. We used a power supply, which could modulate the current in the ten thousandths range and the reaction responded strongly even to the smallest changes of current, which is, probably, due to the same reason.

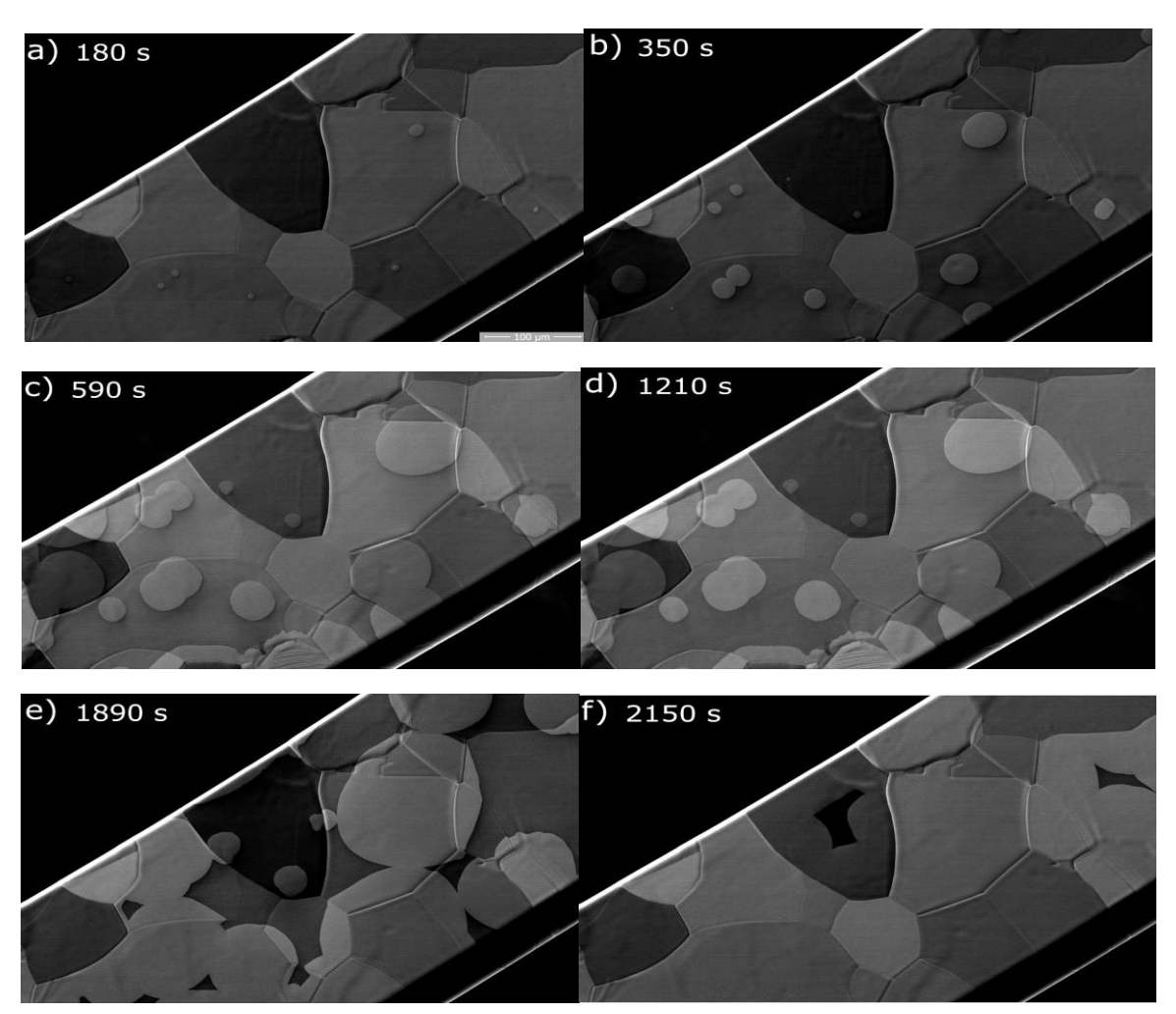


Fig. 2.7: Desorption occurring at reaction conditions, with both CO and O_2 in the chamber, and high temperature (corresponding to I > 1.2 A). This would, eventually, happen over the entire sample. t = 0 s represents the start of desorption.

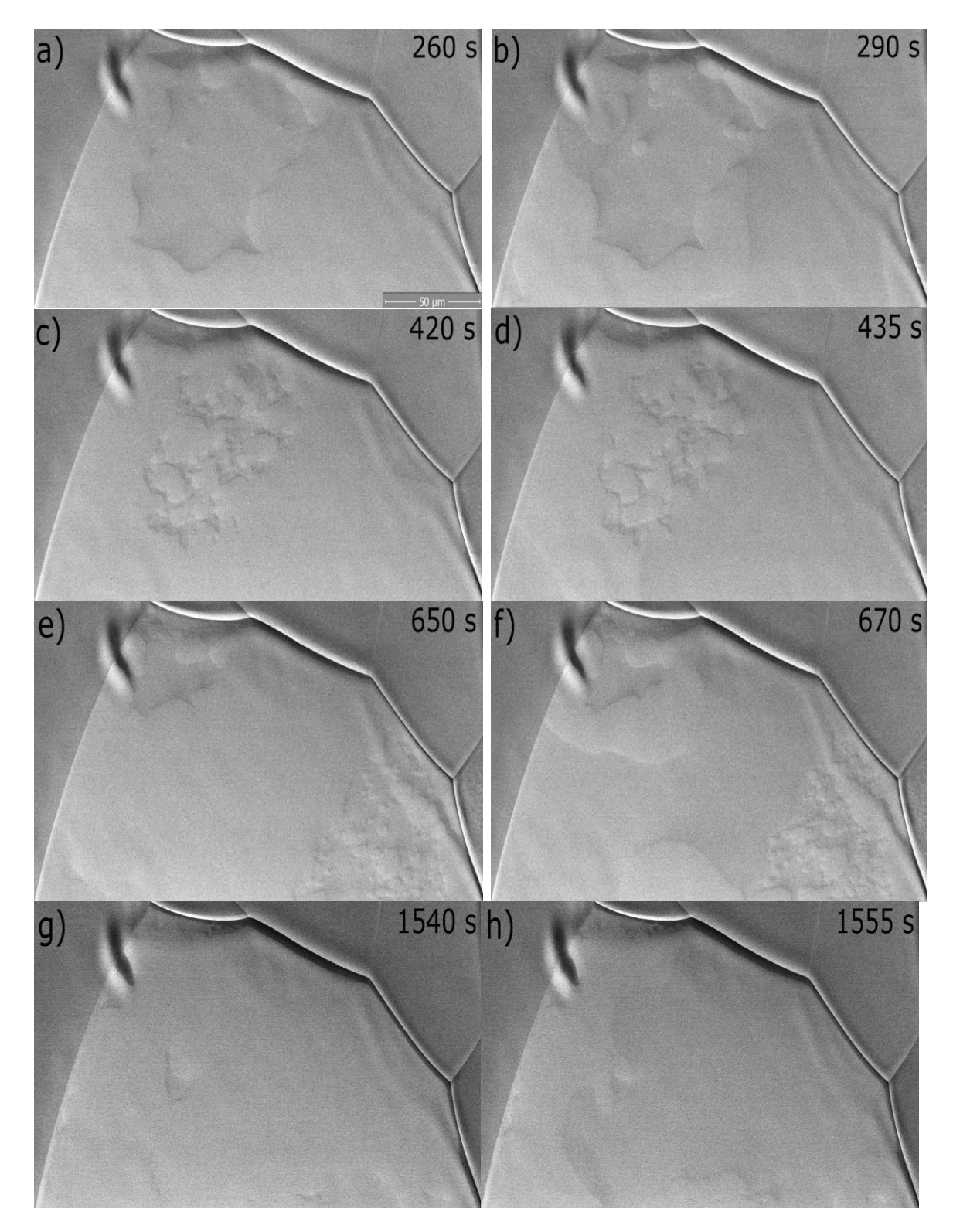


Fig. 2.8: Reaction waves observed in the HV-SEM. The images form pairs, where the first one shows coverage with oxygen and second one shows a passing wave of CO, coming from the edge of the grain (in b) it came from bottom right, in d) as well, in f) it came from bottom left into the middle and in h) it came from bottom right, again). Control parameters: $I=0.8423\,\mathrm{A}$, $p_{\mathrm{CO}}=2.8\cdot10^{-3}\,\mathrm{Pa}$, $p_{\mathrm{O}_2}=1.7\cdot10^{-2}\,\mathrm{Pa}$. $t=0\,\mathrm{s}$ represents time, when reaction conditions were applied, and they remained constant during the reaction.

2.3.2 AFM

In order to be able to use our AFM in the HV-SEM, some technical problems had to be overcome. First of all, the AFM could not be installed directly into the microscope without making any changes to the sample manipulator. An AFM holder had to be made, which fits onto the sample manipulator, onto which the AFM could be attached. Second of all, the AFM scanner cannot withstand temperatures $T > 50 \,^{\circ}\text{C}$, so its temperature had to be monitored by a chromel-alumel thermocouple, which was attached to a multimeter, with which we could read its temperature, which is converted from the voltage difference on the thermocouple. Also, we attached copper wires to the sample holder, as can be seen in Fig. 2.5, to help redirect heat away from the scanner. This was successful, as we confirmed by testing the temperature of the scanner, while heating the sample by a current up to $I = 1.5 \,\mathrm{A}$ and observed no heating of the scanner. Especially, to not damage the scanner by heating the sample to very high temperatures, the cleaning of the sample was done in the UHV-SEM. Additionally, a whole system of flanges, seen on the right side of the microscope in Fig. 2.4, had to be created to accommodate for all the connectors of the AFM and the thermocouple. To set up the AFM for the measurement, often many hours were spent with unscrewing the flanges, inserting the connectors and screwing them back as the AFM could not be stored inside the microscope.

Now, the process of obtaining a CPEM measurement will be described. The CPEM method combines the strengths of an AFM and an SEM to create an image with more information than if the techniques were used independently. At first, we find a spot on the surface with the SEM, which we want to scan. Then, we move the AFM tip to this spot by tracking its movement on the SEM image. We move the electron beam close to the AFM tip, but not too close in order to prevent any interference. Normally, in an SEM, the electron beam scans over the surface, but during CPEM, the AFM scanner moves the sample, which keeps the relative position of the electron beam and the AFM tip the same. Thanks to this, the images from AFM and SEM can be correlated and merged into a new image in post-processing, because they are only displaced by a constant value from each other, by manually choosing a few points in both images, which correspond to the same places on the surface. This image contains information both about the topology of the surface from AFM and the morphology and a bit of chemical composition difference of the surface, due to the different contrast, from SEM. The main advantage of this method is that due to the images being made under the same conditions and in the same place, various correlations, based on the AFM detecting method used, can be made.

Unfortunately, due to various reasons, we did not manage to make the CPEM measurement. We made measurements with the AFM alone, both in atmospheric pressure and vacuum, which partly consisted of modulating the coefficients of the PID control system (in the AFM, only the proportional and integral coefficients are varied). One of the images taken in vacuum of a grain covered with "terraces" can be seen in Fig. 2.9. This image was one of the best we took, as later, problems started appearing. The resolution itself seemed to be enough to maybe observe the boundaries of the reaction waves. However, we had a lot of problems with noise in the AFM measurements, which greatly lowered the quality of the AFM images. Also, there were a lot of technical problems e.g., at one point, the scanner stopped scanning in one direction, which

resulted in an image of only one line on the surface of the sample, which also damaged the surface - creating a groove in the surface due to moving over the line repeatedly (as it was operating in tapping mode). We, eventually, found the problem, but it took quite a while to repair, not leaving us with enough time to try to make the measurement. There was an option to use an AFM from NenoVision called LiteScope, which would maybe be able to perform this measurement, but we decided against it for several reasons. Firstly, our sample holder did not fit in this AFM, as it was too big for it. Secondly, the AFM we used belongs to IPE and we can use it whenever we need to, which was not the case with LiteScope. This could later also lead to installing it in the UHV-SEM. And lastly, we were in the early stages of this experiment, so we needed to test if our solutions, to the technical problems we were facing, would work, and we did not want to damage the much more valued microscope.

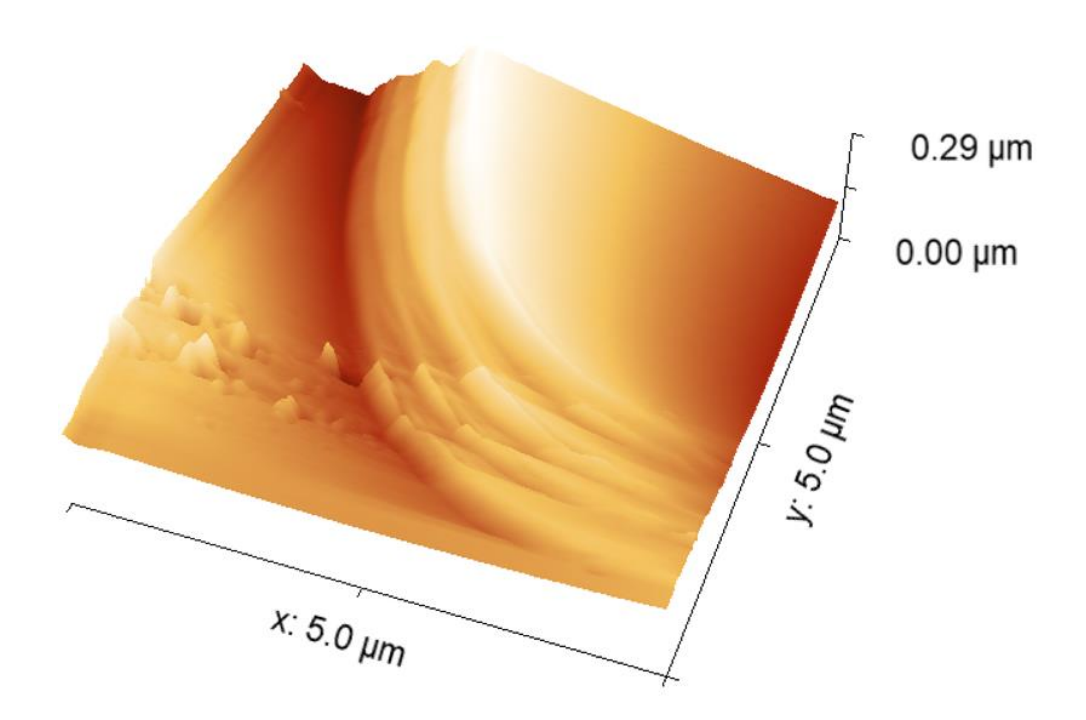


Fig. 2.9: Some of the grains developed "terraces" on them. This is an AFM image of such a grain, taken in vacuum and post-processed in Gwyddion software.

Conclusion

To be able to carry out the observations specified in the goals of this thesis, I mainly had to learn how the scanning electron microscope and the atomic force microscope work, and how to operate them. I successfully managed to do this and later applied this knowledge in the different measurements described in the thesis.

During my work on this thesis, I was successful in completing the goal of observing the reaction waves occurring during the catalytic oxidation of CO on the surface of platinum both in a UHV-SEM and in an HV-SEM in real time. I observed the rate oscillations and different spatiotemporal patterns connected to this reaction. I observed some differences between the two reactions, which are detailed in this thesis.

Unfortunately, the second goal of my thesis, which was to attempt a correlative probe and electron microscopy measurement, combining the powers of the SEM and the AFM, of the reaction waves was not successful. A CPEM measurement of this reaction has never been done before. Understandably so, I faced a lot of problems in trying to make this measurement happen. I, together with Ing. Karel Vařeka and others, have found various solutions and did a lot of work to even be able to operate the AFM in the high-vacuum SEM in the first place. We also did a lot of measurements with the AFM alone, both in atmospheric pressure and in vacuum. However, during our work, we encountered problems, which are further detailed in this thesis, mainly with noise in the AFM images and with the functioning of the AFM itself. This completely prevented us from even trying this measurement.

Moving forward, solutions to the problems, due to which the measurement was not possible, such as noise cancellation or various technical solutions will have to be found, some of which are already being worked on. This could lead to new information, further expanding the knowledge we have of this reaction. Alternatively, different modes of the AFM could be used e.g., measuring force-distance curves, if the obtaining of the topology of the reaction waves will prove to be way more difficult than we previously thought.

References

- [1] VAN SPRONSEN, M. A. et al. Surface science under reaction conditions: CO oxidation on Pt and Pd model catalysts. *Chemical Society Reviews* [online]. 2017, 46(14), 4347-4374 [cit. 2022-05-16]. ISSN 0306-0012 Available at: https://doi.org/10.1039/C7CS00045F
- [2] JEOL ltd. (Japanese Electron Optics Laboratory). Scanning Electron Microscope A To Z [online]. Available at: https://www.jeol.co.jp/en/applications/pdf/sm/sem_atoz_all.pdf
- [3] REIMER, Ludwig. Introduction. In: Ludwig REIMER. Scanning Electron Microscopy: physics of image formation and microanalysis. Second completly revised and updated edition. Berlin: Springer, [1998], Series in Optical Sciences (Springer). p. 1-12. ISBN 978-3-642-08372-3. Available at: doi:10.1007/978-3-540-38967-5 1
- [4] EGERTON, Ray F. The Scanning Electron Microscope. In: Ray F. EGERTON. *Physical Principles of Electron Microscopy*. New York: Springer, 2005, p.125-153. ISBN 978-0387-25800-3. Available at: doi:10.1007/0-387-26016-1_5
- [5] MIRONOV, Victor L. Fundamentals of Scanning Probe Microscopy. Nizhniy Novgorod: Institute of Microstructure Physics, Russian Academy of Sciences, 2004. Available at: http://ipmras.ru/~Mironov/SPM_textbook.html
- [6] BINNIG, G., C. F. QUATE a Ch. GERBER. Atomic Force Microscope. *Physical Review Letters* [online]. 1986, **56**(9), 930-933 [cit. 2022-04-23]. ISSN 0031-9007. Available at: doi:10.1103/PhysRevLett.56.930
- [7] Stylus Profilometry. *Nanoscience Instruments* [online]. Nanoscience Instruments, ©2022 [cit. 2022-05-01].
- Available at: https://www.nanoscience.com/techniques/optical-profilometry/stylus/
- [8] GIESSIBL, Franz J. AFM's path to atomic resolution. *Materials Today* [online]. 2005, **8**(5), 32-41 [cit. 2022-05-01]. ISSN 1369-7021. Available at: doi.org/10.1016/S1369-7021(05)00844-8.
- [9] GUO, Dan et al. Vibration-induced superlubricity. In: Dan GUO et al, eds. *Superlubricity* [online]. Second Edition. Elsevier, 2021, [cit. 2022-05-01], p. 53-70. ISBN 978-0-444-64313-
- 1.Available at: https://www.sciencedirect.com/science/article/pii/B9780444643131 https://www.sciencedirect.com/science/article/pii/B9780444643131
- [10] ALBRECHT, T. R. et al. Frequency modulation detection using highQ cantilevers for enhanced force microscope sensitivity. *J. Appl. Phys.*[online]. 1991, **69**(2),668-673[cit. 2022-05-02]. Available at: doi: 10.1063/1.347347
- [11] IMBIHL, Ronald and Gerhard ERTL. Oscillatory Kinetics in Heterogeneous Catalysis. *Chemical Reviews* [online]. 1995, **95**(3), 697-733 [cit. 2022-05-08]. ISSN 0009-2665. Available at: doi:10.1021/cr00035a012

[12] ERTL, G. Oscillatory Kinetics and Spatio-Temporal Self-Organization in Reactions at Solid Surfaces. *Science* [online]. 1991, **254**(5039), 1750-1755 [cit. 2022-05-08]. ISSN 0036-8075.

Available at: doi:10.1126/science.254.5039.1750

[13] JAKUBITH, S. et al. Spatiotemporal Concentration Patterns in a Surface Reaction: Propagating and Standing Waves, Rotating Spirals, and Turbulence. *Physical Review Letters* [online]. 1990,**65**(24), 3013-3016 [cit. 2022-05-08]. ISSN 0031-9007. Available at: doi:10.1103/PhysRevLett.65.3013

List of abbreviations

3D three-dimensional

AE Auger electrons

AFM atomic force microscopy

AM-AFM amplitude modulation atomic force microscopy

BSE back-scattered electrons

BUT Brno University of Technology

BZ Belousov-Zhabotinsky

CEITEC Central European Institute of Technology

CPEM correlative probe and electron microscopy

CRT cathode-ray tube

FEG field emission gun

FM-AFM frequency modulation atomic force microscopy

HV high vacuum

IPE Institute of Physical Engineering

LCD liquid crystal display

LH Langmuir-Hinshelwood

PE primary electrons

PMT photomultiplier tube

SE secondary electrons

SEG Schottky emission gun

SEM scanning electron microscope

SPM scanning probe microscopy

STM scanning tunnelling microscope

TEG thermionic emission gun

UHV ultra-high vacuum

X X-rays